Microelectronics Reliability 54 (2014) 921–925

Contents lists available at ScienceDirect

Microelectronics Reliability

journal homepage: www.elsevier.com/locate/microrel

Liquid crystal electrography: Electric field mapping and detection of peak electric field strength in AlGaN/GaN high electron mobility transistors

Janina Möreke *, Chris Hodges, Laura L.E. Mears, Michael J. Uren, Robert M. Richardson, Martin Kuball

H.H. Wills Physics Laboratory, Tyndall Avenue, Bristol BS8 1TL, UK

ARTICLE INFO

Article history:
Received 3 October 2013
Received in revised form 6 January 2014
Accepted 7 January 2014
Available online 23 January 2014

ABSTRACT

The liquid crystal mixture E7, based on cyanobiphenyl, has been successfully employed to map electric field strength and distribution in AlGaN/GaN high electron mobility transistors. Using a transmitted light image through crossed polarizers the optical response of the liquid crystal deposited onto the surface of the devices was recorded as a function of source–drain bias, V_{ds}. At a critical voltage of 4 V the preferred direction of orientation of the long axes of the liquid crystal molecules in the drain access region aligned with one of the polarizers resulting in reduced transmitted light intensity. This indicates that at this electric field strength molecule orientation in most of the liquid crystal film is dominated by the electric field effect rather than the influence of surface anchoring. The experimental results were compared to device simulations. Electric field strength above the surface at V_{ds} = 4 V was simulated to reach or exceed 0.006 MV/cm. This electric field is consistent with the field expected for E7 to overcome internal elastic energy. This result illustrates the usefulness of liquid crystals to directly determine and map electric fields in electronic devices, including small electric field strengths.

1. Introduction

AlGaN/GaN high electron mobility transistors (HEMTs) have been the focus of intensive research to deliver improved device reliability in recent years [1]. Their wide bandgap makes them an excellent candidate for high power applications giving improved performance in power-supplies as well as radar or satellite systems. Many aspects of the reliability and operation of these devices are still not very well understood or solved, including the underlying physics of electronic trapping sites within the bulk of the devices [2,3] or within surface leakage paths [4]. In addition, the physical origin of device degradation during operation is still controversial [5,6]. Devices exhibit high internal electric fields and high channel temperatures, well in excess of traditional semiconductor device systems. These can trigger degradation and generation of electronic traps [7]. Investigation techniques employed have included electrical methods [8,9] such as pulsed IV or transient analysis [10,11] as well as optical methods such as electroluminescence [12]. These traps impact device performance including a reduction in source–drain current or can lead to higher leakage currents along interfaces and at the device surface. Typically field plates or gate shaping are used to limit the maximum electric field present in the devices [7]. While accessing temperature in the devices is nowadays easily possible for example using Raman, infra-red or liquid crystal thermography [13–15], quantifying experimentally peak electric fields that drive electronic trap generation and device degradation is challenging. Past efforts have used Kelvin probe force microscopy [16] as well as depth-resolved cathodoluminescence spectra [17] to try to correlate local electric field strength with degradation phenomena due to material defects and stress-induced traps. While liquid crystals have been used in the past to image temperature distribution and hot spots in the devices [18] their potential to image electric fields in electronic devices has been ignored to date. This is despite their wide scale use in displays that exploit their orientation under an electric field [19]. Several different phases of low or high order can be achieved in a liquid crystal depending on temperature or the presence of external electric fields [20]. In this work it is demonstrated that liquid crystal can be used for electric field analysis of electronic devices, on the example of AlGaN/GaN HEMTs. This is done by using their ability to orientate with electric field lines in the nematic phase rather than exploiting a phase change.

2. Experimental details

HEMTs fabricated from a 25 nm AlGaN barrier on a 1.9 μm thick GaN layer grown on an insulating SiC substrate were studied. The

* Corresponding author. Tel.: +44 117 9288750.
E-mail address: Janina.Moereke@bristol.ac.uk (J. Möreke).

0026-2714
http://dx.doi.org/10.1016/j.microrel.2014.01.006

devices were passivated with 325 nm of Si_3N_4. Si_3N_4 is a commonly used layer in the devices to control traps at the surface and device leakage currents [21]. This entire material stack is transparent under white light illumination, apart from areas covered by metal contacts. Source–gate spacing and drain–gate spacing were 1 μm and 2.4 μm, respectively, with a gate length of 0.6 μm and a gate width of 100 μm. Liquid crystal of type E7 were deposited on the HEMT device surface with E7 containing 51% 5CB (cyanobiphenyl), 25% 7CB (cyanobiphenyl), 16% 8OCB (octyloxy-cyanobiphenyl) and 8% 5CT (cyanoterphenyl) [22]. The individual molecules within the mixture have lengths of around 2 nm and demonstrate the nematic phase at a temperature of up to 58 °C. Even though the individual molecules are disordered in the nematic phase, the long axes (as illustrated in Fig. 1C) have a preferred direction. This direction is represented by the director and the material is birefringent. [23] The devices were operated up to a source–drain voltage of 20 V with a gate bias of −6 V. Operating the device under pinch off conditions avoids any significant heating effects. Gate leakage current in the device considered here was less than 0.3 mA/mm. The devices were imaged using an optical microscope with a 50*x*, 0.7 numerical aperture objective, under crossed polarizers with backlight white illumination to record the optical response of the liquid crystal molecules under the electric field in the devices. A schematic of the experimental setup is shown in Fig. 1. For the deposition of the liquid crystal on the AlGaN/GaN HEMT, it is important to achieve a thin layer to avoid convective instabilities [23], which may be caused by temperature or leakage currents. On the other hand, a thin layer on the scale of the dimensions of the liquid crystal molecules would result in alignment dominated by the surface structure or the homeotropic anchoring at the air–liquid crystal interface. For best results a layer below 10 μm was applied, which was found to be thin enough to avoid convective instabilities. This was achieved by applying a droplet of liquid crystal using a needle with the liquid crystal flowing onto the surface of the device due to surface tension, rather than spin-coating. This thickness is consistent with commercially used liquid crystal films for displays [19].

3. Results and discussion

Fig. 2 shows transmitted white light images of the access region for a device at increasing source–drain voltages, V_{ds}, all in pinch-off

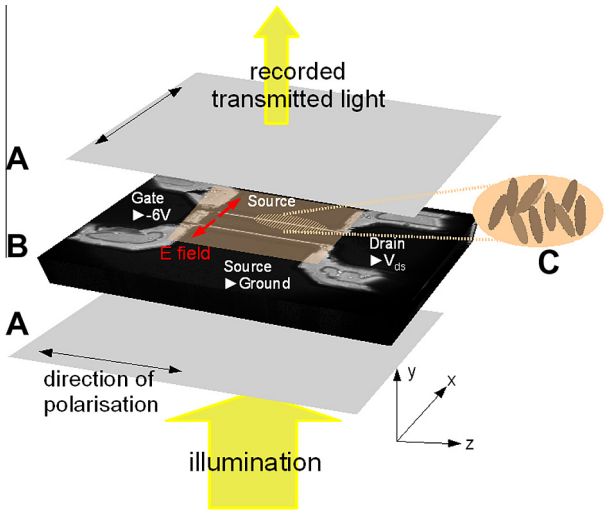

Fig. 1. Schematic set up of measurements showing (A) crossed polarizers with (B) the two gate finger device positioned in between and (C) a representation of liquid crystal.

condition (V_{gs} = −6 V), i.e. no current flow. As the light reaching the camera must pass through crossed polarizers, it can only pass if the optic axis of the nematic is not parallel to either polarizer when no bias is applied to the device. As parts of the device surface are covered by metal contacts only the source–drain access region is visible in the images in Fig. 2. A decrease in light intensity with the increased applied source–drain bias, i.e. with increasing electric field strength, is visible. This decreasing light intensity with applied bias demonstrates the optical response of the orientation of the liquid crystal director, which aligns parallel to the applied electric field and therefore one of the polarizers if enough energy is provided to overcome the effect of surface anchoring of the liquid crystal molecules. As we are operating the device in pinch off no significant heating will affect the liquid crystal film and the darkening of the transmitted light image can be fully attributed to director alignment rather than a phase change in the liquid crystal.

The electric coherence length, ξ_E, [24–26], describes the thickness over which the director orientation is dominated by the elastic forces. Elasticity tends to maintain the director parallel to the surface anchoring. As it is inversely proportional to the electric field strength, it is expected to decrease with increasing source–drain voltage, V_{ds}. A small ξ_E means that only the molecules closest to the device surface will be forced to stay orientated according to surface anchoring leaving the rest free to orientate with the applied electric field. As the electric field is applied parallel to the direction of polarization of one of the polarizers (Fig. 1), alignment of the director with the electric field results in reduced transmitted light. Minimum brightness is achieved when the electric field is sufficiently strong to decrease the value of the electric coherence length to a value that is significantly smaller than the applied liquid crystal film thickness. For an electric field strength of 0.006 MV/cm ξ_E is about 1.6 μm reaching a sub-micron value at an electric field strength of 0.01 MV/cm. We note, the device's own birefringence means that the cross-polarized arrangement always lets some light pass, i.e. even under maximum director alignment (Fig. 2c and d) the images do not become completely dark. Fig. 3 illustrates the average transmitted white light intensity in the active device region as a function of source–drain bias. The intensity values are stated as a fraction of the transmitted light intensity for an unpowered device. The gradual decrease of transmitted light intensity demonstrates the gradual decrease of the electric coherence length. At a source–drain bias of around 4 V (Fig. 2c) the applied electric field dominates over the elastic forces within the liquid crystal and the director is orientated along the direction of polarisation for most of the liquid crystal film. A further increase of the applied voltage, i.e. electric field strength, produces the same director alignment, i.e. the brightness of the images does not decrease any further. As there is no temperature rise in the devices, all changes observed are clearly related to the presence of an electric field in the region where the liquid crystal is situated.

Drift diffusion simulations of the AlGaN/GaN HEMT were performed using Silvaco ATLAS to determine the strength of the electric field at the critical voltage that resulted in reorientation of the majority of the liquid crystal molecules with the electric field. Fig. 4 shows the result of the simulation at a source–drain voltage of 3 V, slightly below the experimentally observed voltage of director alignment of 4 V. Fig. 4a considers the typical scenario of air above the Si_3N_4 passivation while Fig. 4b shows the experimental case with the liquid crystal on top of the Si_3N_4 passivation. The liquid crystal layer was simulated up to a thickness of 3 μm as the electric coherence length will lie within this thickness. Liquid crystal molecules above this thickness will be able to orientate freely with an external applied field due to the absence of a strong surface anchoring effect of the underlying hard surface and hence have no strong impact on the observed effect. The weak boundary

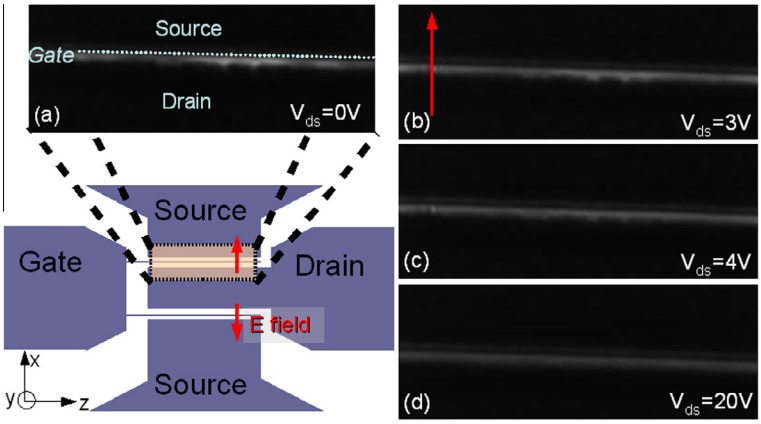

Fig. 2. Transmitted light images of (a) an unpowered AlGaN/GaN HEMT device, (b) biased at V_{ds} = 3 V, (c) at V_{ds} = 4 V and (d) at V_{ds} = 20 V, all at pinch off (i.e. V_{gs} = −6 V).

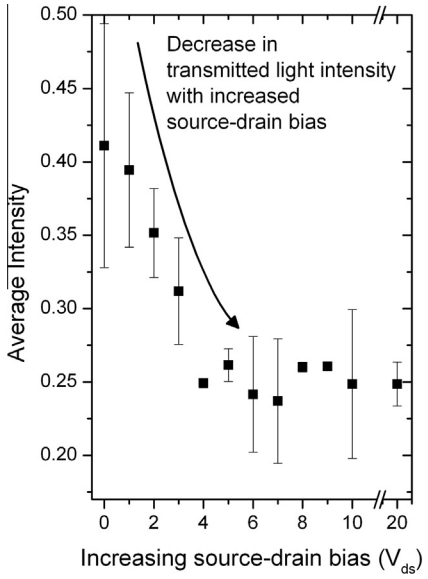

Fig. 3. Average light intensity transmitted through source–drain device region as a function of source–drain bias.

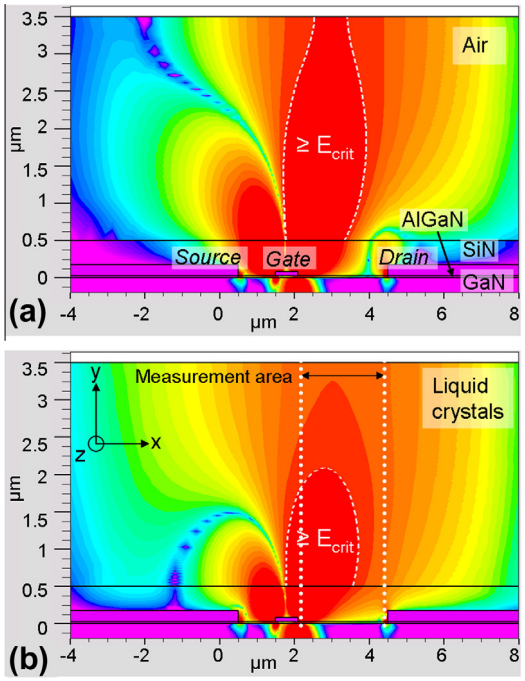

Fig. 4. Lateral component (X) of the electric field in the AlGaN/GaN HEMT from source to drain contact at V_{ds} = 3 V, V_{gs} = −6 V with (a) air above the Si_3N_4 passivation and (b) material with dielectric constant consistent with that for liquid crystals aligned horizontally with the electric field. The area in between dotted straight white lines in (b) shows the area that is being recorded for transmitted light images.

effect between air and liquid crystal has not been found to dominate in the unpowered state as such a boundary causes homeotropic, i.e. light blocking, orientation of the director. It will therefore also not dominate in the powered state and most of the molecules above the simulated thickness are able to orientate easily with the electric field. The peak electric field is present as expected near the gate contact on its drain side. The presence of the liquid crystal compared to air above the Si_3N_4 passivation layer was found to have negligible impact on the electric field strength at the gate edge or in the most part of the Si_3N_4 passivation layer. The technique does not alter the electric field significantly within the device. Fig. 5 displays the lateral electric field strength taken vertically through the AlGaN, SiN and liquid crystal layers. This cross section was taken by the drain-side edge of the gate metal demonstrating therefore the change in peak electric field at this point. The peak electric field near the gate contact determines how the devices operate, i.e. their current–voltage (IV) characteristics, and also impacts and is of key relevance for device degradation mechanisms. The lateral component (X) of the electric field is presented in Fig. 4 as it is this component that represents the main contribution to the total field at the site where the liquid crystal is located. This will cause orientation of the director horizontally from source to drain contact and not vertically.

Rotation of the polarizers in the experiment above the critical voltage of 4 V changed the light intensity consistent with liquid crystal director being horizontally orientated. Vertical orientation would not result in any intensity changes as such material is effectively not birefringent. Due to the liquid crystal's anisotropy, its dielectric constant differs depending on the orientation of the director with the electric field, from a value of around 7 for when the director points perpendicular to the field, i.e. the long axes of the liquid crystal molecules are statistically mainly orientated perpendicular to the field and 18 for parallel orientation. In the simulation a high dielectric constant material was chosen to consider the director pointing horizontally as experimentally observed. Experimental results indicate that the field strength required to orientate the director parallel with the direction of polarization, needs to be reached in the lateral electric field component (X) in the devices.

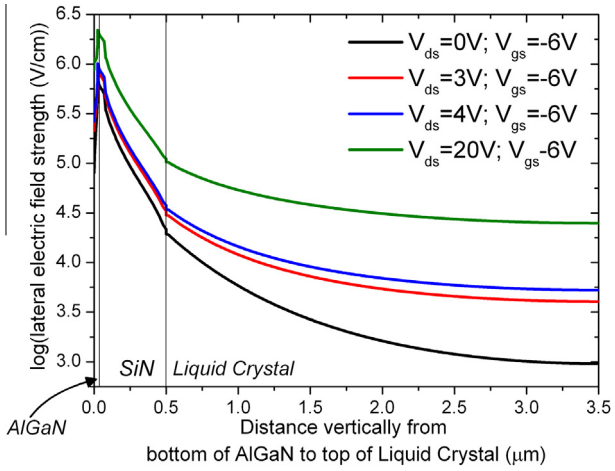

Fig. 5. Log of lateral component (X) of the electric field in the AlGaN/GaN HEMT taken vertically from the bottom of the AlGaN layer past the drain-side edge of the gate metal and through the liquid crystal layer for source drain biases of 0 V (black), 3 V (red), 4 V (blue) and 20 V (green) all at pinch off. (For interpretation of the references to colour in this figure legend, the reader is referred to the web version of this article.)

We note, that the dielectric constant of the liquid crystal along the molecules' short axes (i.e. director orientation perpendicular to the electric field) is only 7. The surface electric field for orienting liquid crystal molecules vertically to the device surface would therefore be significantly higher than parallel to the device surface. The white dashed line in Fig. 4 encircles the area above the Si_3N_4 passivation, in which the electric field exceeds or is equal to an electric field strength of 0.006 MV/cm. In Fig. 6 the electric field strength in the source–drain region is plotted at 2.125 μm above the Si_3N_4 surface. At 4 V the area in which an electric field strength of 0.006 MV/cm is reached or exceeded can be seen to increase covering close to all of the drain access region and therefore the measurement area. As previously stated the electric coherence length is reduced to 1.6 μm at this field strength, leaving a large portion of the liquid crystal film to orientate with the electric field. Such an electric field strength has also been reported in previous work on experiments to find field strength needed to orientate the liquid crystal director between two hard surfaces [19,27] with a gap of 3 μm. Despite depending on the gap size for the definition of a threshold electric field these works demonstrate the investigation of the same balance of forces than in the present work looking at the electric

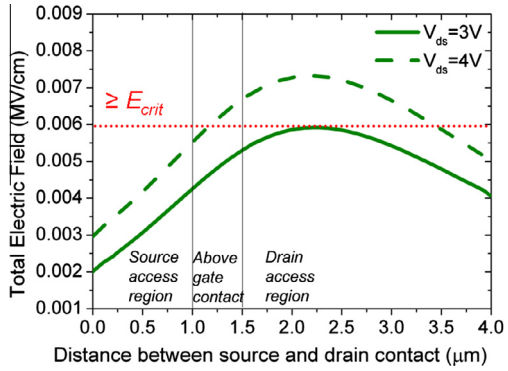

Fig. 6. Simulated total electric field strength in the access regions at a distance of 2.125 μm above the Si_3N_4 surface illustrating expansion and increase of electric field strength in the drain access region with increasing V_{ds}. The dotted red line indicates the critical electric field strength of 0.006 MV/cm. (For interpretation of the references to colour in this figure legend, the reader is referred to the web version of this article.)

coherence length on the surface of an AlGaN/GaN HEMT, i.e. the elastic energy within the liquid crystal needs to be overcome to orientate molecules. Previous work has focused on measuring the optical response of liquid crystal under an external electric field without an underlying structure such as a HEMT [28,29]. Those results confirm the correlation between light transmission and orientation of the liquid crystal relative to the direction of polarization and therefore form calibration data for applying the concept on a structure such as a HEMT.

The results and good agreement of experiment with simulation and theory illustrate that liquid crystals can successfully be used to map electric fields in electronic devices. Their high sensitivity to electric fields means that even small fields can be detected. As the surface of the devices is probed in the experiment, comparison to device simulations is beneficial to correlate to the larger peak electric fields at the gate edge in the devices. The experimental approach can identify location of field concentrations or identify the absence of expected field concentrations due to presence of undiagnosed surface leakage paths. This approach would provide a very useful tool for lifetime testing to observe electric field induced degradation. Different liquid crystals can be employed with different threshold voltages to sense different electric fields, in a similar way to that previously used in terms of thermal transition temperatures in liquid crystal thermography as response to temperature and external electric fields varies depending on the type of liquid crystal. For instance the cyanobiphenyl based liquid crystal 5CB as well as a polymer based liquid crystal have been shown to respond to electric fields of the strength of 0.002 MV/cm, i.e. at smaller electric fields than the liquid crystal mixture E7 used here (0.006 MV/cm) and could therefore be used to probe even smaller electric fields than demonstrated here. Temperatures at which the liquid crystal displays the nematic phase vary from room temperature for E7 or 5CB, to a range of 131–240 °C for 5CT and below 35.1 °C for the polymer based liquid crystal [30,20,22]. A liquid crystal displaying the nematic phase is needed for the technique demonstrated here to work, so as long as the device stays in the temperature range for the nematic phase, the technique can also be applied to operation with open channel rather than only the pinched off condition demonstrated here.

4. Conclusions

A method to map electric fields and determine electric field strength in electronic semiconductor devices, liquid crystal electrography, was developed. Use of liquid crystals under crossed polarizers can be employed to determine bias voltages that result in critical electric field strengths at the device surface. Even small field strengths can be detected with this method. This was illustrated on AlGaN/GaN HEMTs passivated with Si_3N_4. The electric field on the Si_3N_4 surface affects the alignment of a thin film of liquid crystal molecules by orientating the director with the electric field.

Acknowledgement

We acknowledge financial support from the Engineering and Physics Sciences Research Council (EPSRC) under EP/H037853/1.

References

[1] Delage SL, Dua C. Wide band gap semiconductor reliability: status and trends. Microelectron Rel 2003;43:1705–12.
[2] Arehart AR, Sasikumar A, Rajan S, Via GD, Poling B, Winningham B, et al. Direct observation of 0.57 eV trap-related RF output power reduction in AlGaN/GaN high electron mobility transistors. Solid State Electron 2013;80:19–22.

[3] Astre G, Tartarin JG, Lambert B. Trapping related degradation effects in AlGaN/GaN HEMT. In: Proceedings of 5th Europ. Microwave Integrated Circuit Conf (2010):298–301.
[4] Kim H, Thompson RM, Tilak V, Prunty TR, Shealy JR, Eastman LF. Effects of SiN passivation and high-electric field on AlGaN–GaN HFET degradation. IEEE Electron Device Lett 2003;24:421–3.
[5] Chowdhury U, Jimenez JL, Lee C, Beam E, Saunier P, Balistreri T, et al. TEM observation of crack-and pit-shaped defects in electrically degraded GaN HEMTs. IEEE Electron Device Lett 2008;29:1098–100.
[6] Montes Bajo M, Hodges C, Uren MJ, Kuball M. On the link between electroluminescence, gate current leakage, and surface defects in AlGaN/GaN high electron mobility transistors upon off-state stress. Appl Phys Lett 2012;101. 033508 (4 pages).
[7] Möreke J, Ťapajna M, Uren MJ, Pei Y, Mishra UK, Kuball M. Effects of gate shaping and consequent process changes on AlGaN/GaN HEMT reliability. Phys Status Solidi (a) 2012;209:2646–52.
[8] Silvestri M, Uren MJ, Kuball M. Iron-induced deep-level acceptor center in GaN/AlGaN high electron mobility transistors: energy level and cross section. Appl Phys Lett 2013;102. 073501 (4 pages).
[9] Meneghesso G, Rampazzo F, Kordoš P, Verzellesi G, Zanoni E. Current collapse and high-electric-field reliability of unpassivated GaN/AlGaN/GaN HEMTs. IEEE Trans Electron Devices 2006;53:2932–41.
[10] Uren MJ, Möreke J, Kuball M. Buffer design to minimize current collapse in GaN/AlGaN HFETs. IEEE Trans Electron Devices 2012;59:3327–33.
[11] DasGupta S, Sun M, Armstrong A, Kaplar RJ, Marinella MJ, Stanley JB, et al. Slow detrapping transients due to gate and drain bias stress in high breakdown voltage. Trans Electron Devices 2012;59:2115–22.
[12] Hodges C, Killat N, Kaun SW, Wong MH, Gao F, Palacios T, et al. Optical investigation of degradation mechanisms in AlGaN/GaN high electron mobility transistors: generation of non-radiative recombination centers. Appl Phys Lett 2012;100. 112106 (4 pages).
[13] Pomeroy J, Gkotsis P, Zhu M, Leighton G, Kirby P, Kuball M. Dynamical operational stress measurement of MEMS using time-resolved Raman spectroscopy. J Micromech Syst 2008;17:1315–21.
[14] Berthet F, Guhel Y, Gualous H, Boudart B, Trolet JL, Piccione M, et al. Characterization of the self-heating of AlGaN/GaN HEMTs during an electrical stress by using Raman spectroscopy. Microelectron Rel 2011;51:796–1800.
[15] Batten T, Manoi A, Uren MJ, Martin T, Kuball M. Temperature analysis of AlGaN/GaN based devices using photoluminescence spectroscopy: challenges and comparison to Raman thermography. J Appl Phys 2010;107. 074502 (5 pages).
[16] Wakejima A, Ota K, Nakayama T, Ando Y, Okamoto Y, Miyamoto H, et al. Observation of cross-sectional electric field for GaN-based field effect transistor with field-modulating plate. Appl Phys Lett 2007;90:213504.
[17] Lin C-H, Merz TA, Doutt DR, Joh J, del Alamo J, Mishra UK, et al. Strain and temperature dependence of defect formation at AlGaN/GaN high electron mobility transistors on a nanometer scale. IEEE Trans Electron Devices 2012;59:2667–74.
[18] Babić DI, Diduck Q, Smart J, Francis D, Faili F, Ejeckam F. Measurement of thermal boundary resistance in AlGaN/GaN HEMTs using liquid crystal thermography. MIPRO 2012:48–53.
[19] <http://www.fujitsu.com/downloads/MICRO/fma/pdf/LCD_Backgrounder.pdf> Fujitsu white paper on liquid crystal displays [accessed 15.08.13].
[20] Cairns DR, Shafran MS, Sierros KA, Huebsch WW, Kessman AJ. Stimulus-responsive fluidic dispersions of rod shaped liquid crystal polymer colloids. Mater Lett 2010;64:1133–6.
[21] Green BM, Chu KK, Chumbes EM, Smart JA, Shealy JR, Eastman LF. The effects of surface passivation on the microwave characteristics of undoped AlGaN/GaN HEMTs. IEEE Electron Device Lett 2000;21.
[22] Raynes EP, Tough RJA, Davies KA. Voltage dependence of the capacitance of a twisted nematic liquid crystal layer. Mol Cryst Liq Cryst 1979;56:63–8.
[23] Collings PJ, Hird Michael. Introduction to liquid crystals. 1st ed. London (UK): Taylor & Francis Ltd; 1998.
[24] de Gennes PG, Prost J. The physics of liquid crystals. 2nd ed. Oxford (UK): Oxford University Press; 1993.
[25] Nobili M, Durand G. Disorientation-induced disordering at a nematic-liquid-crystal–solid interface. Phys Rev A 1992;46:6174–7.
[26] Dhara S, Madhusudana NV. Influence of director fluctuations on the electric-field phase diagrams of nematic liquid crystals. Europhys Lett 2004;67:411–7.
[27] Tsai T-Y, Huang Y-P, Chen H-Y, Lee W, Chang Y-M, Kuo Chin W-. Electro-optical properties of a twisted nematic–montmorillonite–clay nanocomposite. Nanotechnology 2005;16:1053–7.
[28] Lee SH, Lee SL, Kim HY. Electro-optical characteristics and switching principle of a nematic liquid crystal cell controlled by fringe-field switching. Appl Phys Lett 1998;73:2881.
[29] Yeh Pochi, Claire Gu. Optics of liquid Crystal displays. 2nd ed. Hoboken, New Jersey (USA): John Wiley & Sons Inc.; 2010.
[30] Alexander GG, Cubitt R, Dalgliesh RM, Kinane C, Richardson RM, Zimmermann H. A neutron reflection study of surface enrichment in nematic liquid crystals. Phys Chem Chem Phys 2011;32:14784–94.